MATEC Web of Conferences **119**, 01003 (2017) DOI: 10.1051/matecconf/201711901003
IMETI 2016

Analysis and optimization of a novel linear permanent Vernier motor

Yi Shao[a], Degang Lv and Ying Xie

School of Electrical and Electronic Engineering, Harbin University of Science and Technology, China

Abstract. In this paper, a novel linear permanent magnet vernier (LPMV) motor is proposed. The advantages of the proposed motor are high force density, high efficiency, simple structure, and low cost. Firstly, the structure and the operation principle of the proposed motor which adopts 12-slots-11-pair-poles structure are descried. Based on the air-gap permeance function, the components of air-gap flux density is discussed. Secondly, the validation of LPMV is analyzed by finite element method (FEM), and the basic electromagnetic performance such as air-gap flux density, back-EMF, detent force and thrust waveform are analyzed in detail. Finally, the relationship between the thrust force characteristics and the design parameters are analyzed to provide useful information to the designers of LPMV.

1 Introduction

Compared with conventional permanent magnet motors, the direct-drive permanent magnet motors have a lot of advantages. With the absence of a reduction gear, the problems, such as backlash, friction loss, and maintenance can be eliminated. In addition, to some extent, the complexities and failure possibility of the system can be lowered, thus, the reliability and efficiency are enhanced.
A coaxial magnetic gear has been proposed as a type of direct drive technology, which offers a high thrust density. However, the integrated machines employ two or more moving parts with multiple air-gaps; thus, they suffer from manufacture difficulty. To circumvent this problem, a new class of linear machines based on the field modulation principle of the magnetic gear, known as vernier machines, was introduced.

PMV motor was firstly proposed in 1995 by A. Ishizak. It made clear that the PMV motor can obtain high thrust at low speed and the steady thrust equation was derived in [1].Then, Toba and Lipo presented comprehensive design considerations of surface PMV motor for pursuing thrust maximizing [2]. After that various new PMV topologies have been proposed to further improve thrust density. In [3, 4], both the thrust density and power factor of the PMV motors has been improved by employing spoke magnets. In recent years, Vernier PM motor is attracting more and more attention due to their simple mechanical structure, high torque density, sinusoidal back electromotive force (EMF) waveform, and low pulsation ripple [5-11].

Contrasted with the traditional transmission way, the linear motor is omitted mechanical transmission part. And linear motor has simple structure, and there is no direct contact between mover and stator. So it has a low friction, low noise and long working life. The characteristic of high

[a] Corresponding author : 18645140103@163.com

precision can be easily achieved by the corresponding control method. So the linear motor is widely used in industrial processes, transportation, etc. For a variety of linear drive applications, high force density is essential.

As the rotation Vernier permanent magnet motors are investigated widely around the world, the research of VPM which is employed in linear machine field is few. By extending the idea to linear topology, a novel LPMV machine, which can offer simple structure and high force density, is proposed and analyzed in this paper. In order to analyze the electromagnetic performance, such as the thrust density, the thrust ripple, the detent force, etc., the influence of and some design parameters, such as the stator/rotor pole number, the slot opening ratio, the magnet thickness, the excitation current, etc. The performance will be fully investigated by finite-element analysis (FEA) in detail [12-17].

2 Structure and working principle of linear permanent magnet Vernier motor

2.1. Structure of linear permanent magnet Vernier motor

Fig.1 shows the topology of proposed LPMV motor. The long stator is made of simple iron core and permanent magnets (PM),and the PM is surface mounted on the stator. The mover is consisted of excitation winding and iron core.

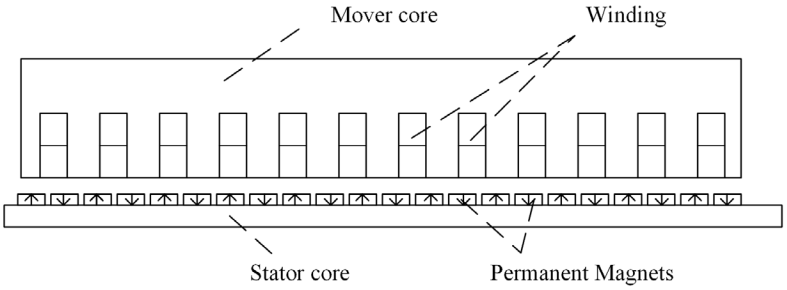

Figure 1. The novel linear permanent magnet vernier motor.

Different with regular PM machines, the slots and tooth of the stator for VPM machine are not only for embedding windings or serving as a part of the magnetic path, but also working as flux modulators, which has a significant influence on thrust performance of VPM machines. In order to maintain the same modulation effect along radial direction of a VPM machine, trapezoidal slot is desirable since the ratio of slot opening width to slot pitch remains constant. However, due to manufacturing difficulties, a radially proportional structure for an axial flux machine may not be a cost-effective option when silicon steel sheet are used to fabricate iron cores. Therefore, rectangular instead of trapezoidal slots are chosen for the proposed machine. On the rotor side, trapezoidal shaped magnets are preferred to keep the pole are unchanged and thus remain a balanced magnetic loading along radial direction.

2.2 Principle of linear permanent magnet Vernier motor

Stator coils with concentrated windings are excited by a three-phase balanced sinusoidal current and generate a travelling magnetic field. The magnetomotive force (MMF) of the A-phase can be expressed in the following equations:

$$F_{ca} = \frac{4\sqrt{2}NI}{\pi p}\sum_{m}\left\{\frac{1}{m}g_u(\mathrm{m})\sin(mp\theta)\sin(\omega \mathrm{t})\right\} \tag{1}$$

$$g_u(m) = \sin\frac{m}{2}\pi\cdot\sin\frac{m}{6}\pi \tag{2}$$

Where N is the number of coil turns in each phase, I is the of sinusoidal coil current (effective value),p is the pole pairs of the travelling magnetic field, θ is the mechanical angle, and m is a positive odd number. The angular velocity ω is equal to $2\pi f$,where f is the frequency of the sinusoidal current.

$$F_c = F_0\sum_{l}\left[\frac{1}{6l+1}g(l)\cos\{\omega t-(6l+1)p\theta\}\right] \tag{3}$$

$$F_0 = \frac{6\sqrt{2}NI}{\pi p} \tag{4}$$

$$g(l) = \sin\frac{6l+1}{2}\pi\cdot\sin\frac{6l+1}{2}\pi \tag{5}$$

where l is an integer $(l = 0,\pm1,\pm2,\pm3)$

The permeance of the stator teeth can be expressed in the following equation:

$$P_{sm} = P_{s0} + \sum_{m} P_{sm}\cos(mZ_1\theta) \tag{6}$$

Where P_{sm} is the amplitude of the permeance of the mth harmonic,Z_1 is the number of stator teeth. However,(6) can be simplified using its major components, and can be expressed as follows:

$$P_{s1} = P_{s0} + P_{s1}\cos(Z_1\theta) \tag{7}$$

Consequently the multiplication of (3) and (7) yields the flux density distribution

$$B_{sl} = F_c P_{s1} = F_0\sum_{l}\left\{\frac{1}{6l+1}g(l)\cos(\omega t-(6l+1)p\theta)\right\}\times\{P_0+P_1\cos(Z_1\theta)\} \tag{8}$$

The major components $(l = 0,\pm1,\pm2,\pm3)$ of the flux density distribution are expanded and shown below:

$$B_{s(0)} = F_0P_0g(0)\cos(\omega t-p\theta)+\frac{F_0P_1g(0)}{2}\left[\cos\{\omega t+\theta(Z_1-p)\}+\cos\{\omega t-\theta(Z_1+p)\}\right] \tag{9}$$

$$B_{s(-1)} = \frac{F_0P_0g(-1)}{5}\cos(\omega t+5p\theta)+\frac{F_0P_1g(-1)}{5}\left[\cos\{\omega t+\theta(Z_1+5p)\}+\cos\{\omega t-\theta(Z_1-5p)\}\right] \tag{10}$$

$$B_{s(+1)} = \frac{F_0P_0g(1)}{7}\cos(\omega t-7p\theta)+\frac{F_0P_1g(1)}{7}\left[\cos\{\omega t+\theta(Z_1-7p)\}+\cos\{\omega t-\theta(Z_1+7p)\}\right] \tag{11}$$

$$B_{s(-2)} = \frac{F_0 P_0 g(-2)}{11}\cos(\omega t + 13p\theta) + \frac{F_0 P_1 g(-2)}{11}\left[\cos\{\omega t + \theta(Z_1 + 11p)\} + \cos\{\omega t - \theta(Z_1 - 11p)\}\right] \quad (12)$$

$$B_{s(+2)} = \frac{F_0 P_0 g(2)}{13}\cos(\omega t - 13p\theta) + \frac{F_0 P_1 g(2)}{13}\left[\cos\{\omega t + \theta(Z_1 - 13p)\} + \cos\{\omega t - \theta(Z_1 + 13p)\}\right] \quad (13)$$

In this paper, $Z_1 = 12$ and $p = 1$ are chosen. Therefore the second term (9) and the first term (12) generate the 11th flux harmonic, which travels in the opposite direction of the fundamental rotating magnetic field at 1/11 times the speed. At the same time, the third term(13) and the first term (9) generate the 13th flux harmonic, which travels in the same direction of the fundamental rotating magnetic field at 1/13 times the speed. The mover will synchronize with the 11th or 13th flux harmonic if the number of permanent magnet pole pairs chosen is 11 or 13.

As mentioned in the previous section, the mover of the vernier motor synchronizes with the flux harmonics of the magnetic field and rotates with a reduction ratio with respect to the angular velocity of the magnetic field.

Therefore in order to operate correctly, the following structural relationship shown in(14) between Z_1, p, and Z_2 has to be satisfied. The rotor will then rotate at ω_m , which is an angular velocity with a reduction ratio of p/Z_2 of the synchronous velocity ω /p,and is expressed in (15).

$$Z_2 = Z_1 \pm p \quad (14)$$

$$\omega_m = \frac{\omega}{p} \times \frac{p}{Z_2} = \frac{\omega}{Z_2} \quad (15)$$

3 Model validation

In order to verify the forgoing analysis about proposed LPMV, a finite element model is built and investigated by Maxwell_2D, the main design parameters of proposed motor are tabulated in table I and the structure of proposed LPMV is shown in Fig 2.

Table 1. Setting Word's margins.

Symbol	Parameter
Mover width	132mm
Mover pole pitch h_c	11mm
Mover Slot Width h_c	4.8mm
Mover Slot Depth g_c	6mm
PM thickness g_m	2.3mm
PM width h_m	4.8mm
Number of Slot/Pitch	12/22
Magnet material	NdFe35
Current Density	6A/mm^2
Thrust	235N
Mover Speed	1m/s
Each slot number of conductor	25
Air-gap length	1mm

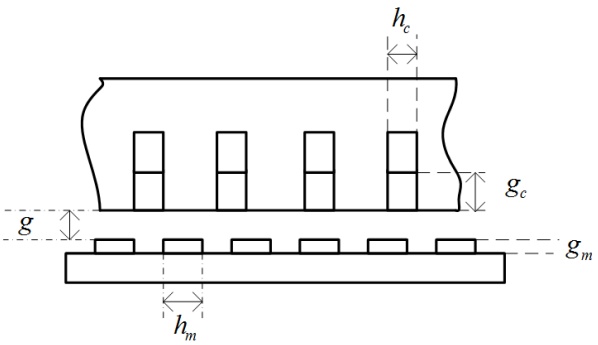

Figure 2. The simplified structure of proposed motor.

3.1 Magnetic field distribution

Fig 3. shows the magnet flux plot of a VPML machine at a different angle position, and it can be seen that the small rotor position displacement introduces a large flux variation. VPML machine has a same operation principle with magnetic gear motor which is called as “magnetic gear effects”.

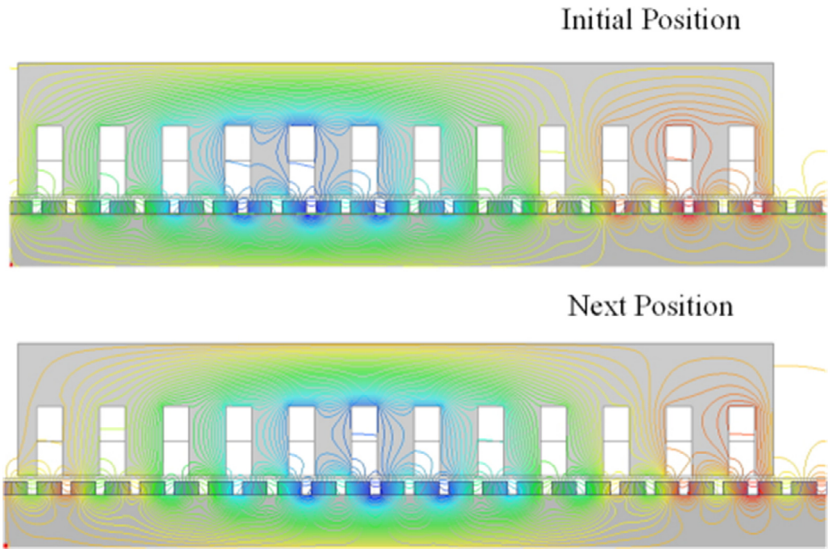

Figure 3. The magnetic field distributions of proposed motor

3.2 Air-gap flux density

The air-gap flux density waveform of the proposed VPML machine only due to PM is shown in Fig 4. It can be seen the maximum flux density of the proposed motor is 0.55T, and the harmonic analysis is done by Fast Fourier Transformation (FFT) as shown in Fig 5. the largest component of air-gap flux density is 0.29T of 11th harmonic. Respectively,Fig.5 shows the corresponding space harmonic spectrum. Obviously,the 11th harmonic makes the maximum.

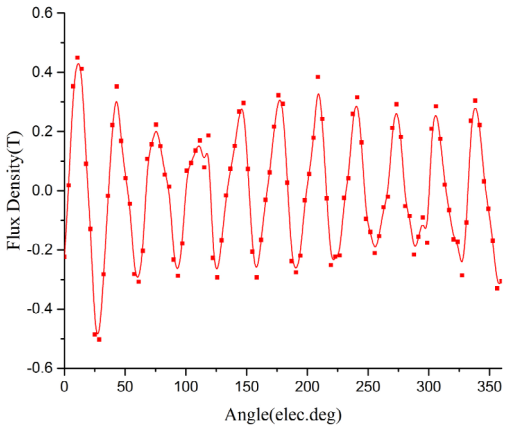

Figure 4. The Air-gap flux density distribution of proposed motor.

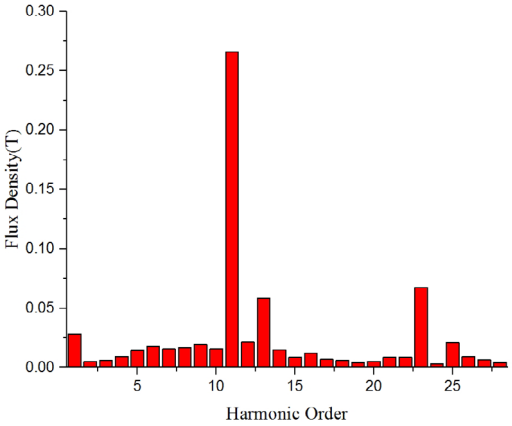

Figure 5. The corresponding space harmonic spectrum of proposed motor.

3.3 No-load Back-EMF and force characteristic

The no-load back-EMF waveform of the proposed motors at nominal speed of 1m/s is shown in Fig 6. the phase angle between a, b, and c is 120o, however, the amplitude of a is 76.7V, and it is smaller than 75.2Vof b and c, which is the result of end effect in the linear machine.

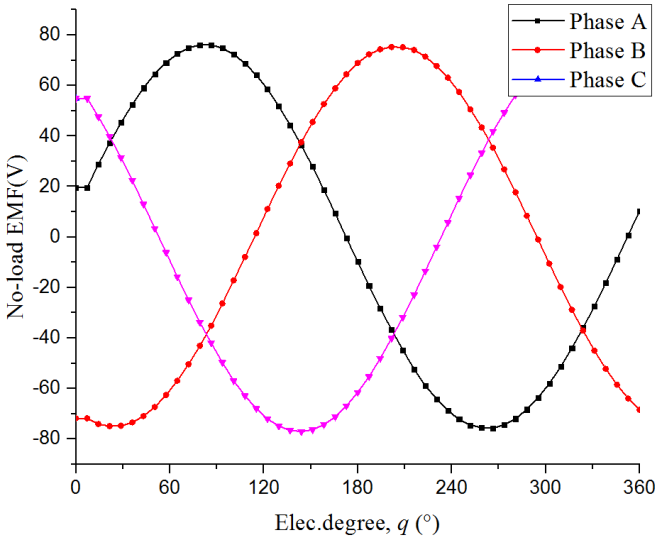

Figure 6. The no-load back-EMF waveform of the proposed motor.

Fig 7. Shows the characteristic of the thrust force and cogging force, and the average thrust is 235N, the thrust ripple is 7%. The thrust ripple includes detent force, cogging force and friction, and the amplitude of cogging force is 5.1N.

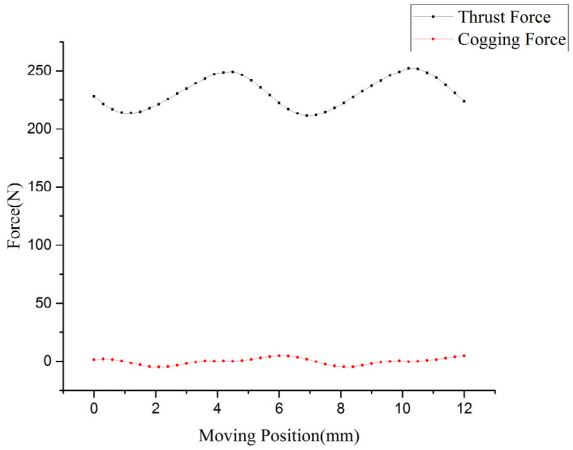

Figure 7. The force characteristic of the proposed motor.

4 Parameter analysis and its determination

In this section, the influence of several geometrical and physical parameters on the thrust force is investigated to provide useful information for the designers of permanent magnet vernier linear motor.

4.1 Influence of the air gap length

Fig 8 shows the thrust force characteristic with different air gap lengths. It can be seen that the thrust decreases gradually as the air gap increases, and this is a result of lower magnetic density under larger air gap length. When the air-gap length is 2mm, the amplitude of 11th harmonic of air-gap flux density is 1.38T, that is approximately 1/2 of the one under 1mm air-gap; the average thrust is 112 N, that is 1/2 of the one under 1mm air-gap.

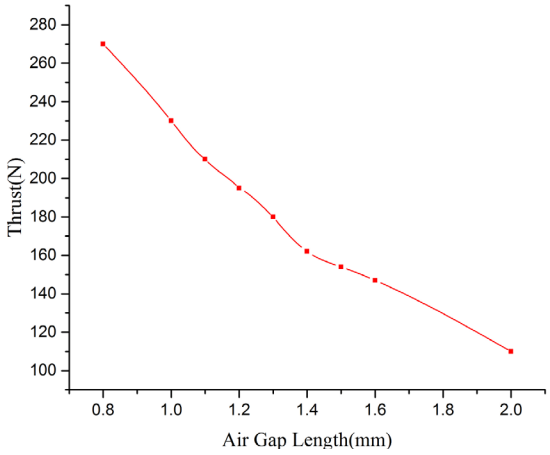

Figure 8. The thrust force characteristic with different air gap length.

4.2 Influence of the magnet dimension

The effect of the two magnet dimensions: the width of the permanent magnets h_m and the height of the permanent magnets b_m, are analyzed. The study is performed under the consideration of constant magnet volume. The pole-arc coefficient is calculated by:

$$\alpha = \frac{h_m}{\tau} \tag{16}$$

where τ is the pole pitch.

The pole-arc coefficient has an important influence on the air gap flux density waveform by changing the percentage of 11th harmonic which can significantly influence the average thrust. Meanwhile, the pole-arc coefficient also influences the thrust ripple. The analysis result is shown in Fig 9, the thrust is increased with the decrease of pole-arc coefficient, from 14 N under α =0.65 to 20N under α=0.9; the thrust ripple reaches the minimum value of 7% when α =0.8.

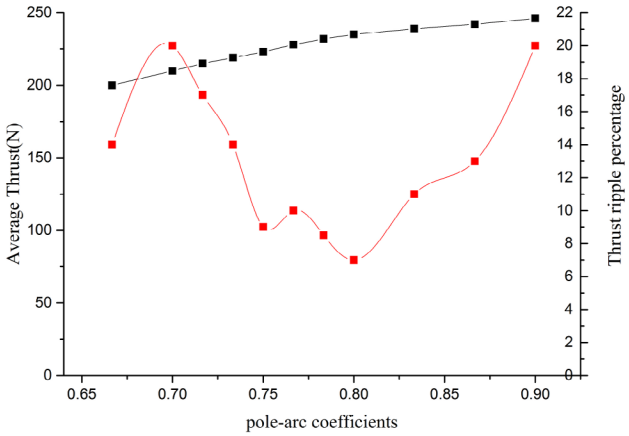

Figure 9. The thrust force characteristic with different pole-arc coefficients.

4.3 Influenced of the slot-opening factor

The slot-opening factor influences the distribution function of air-gap permeance, then influences the detent force and thrust ripple of motor. The analysis of slot-opening factor is done under the condition of same slot-area and slot-filling factor. From Fig 10, the thrust ripple is increased with the increasing of slot-opening factor when the current density is small as 6A/mm^2 and 12A/mm^2; then the thrust ripple is decreased with the increasing of slot-opening factor when the current density is 18A/mm^2, that is the result of saturation effect in the teeth part.

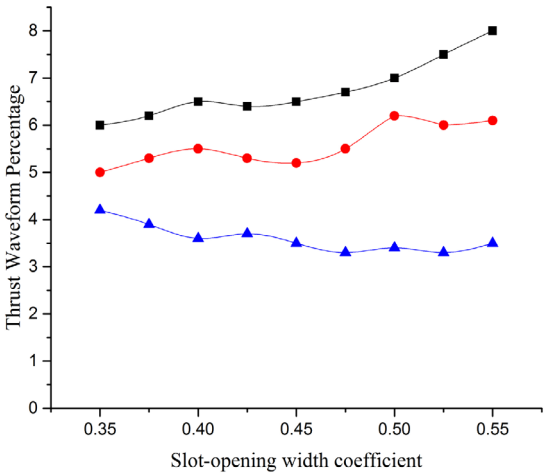

Figure 10. The thrust ripple with different slot-opening width coefficient.

4.4 Influenced of the excitation current

The curve of thrust versus current density is shown in Fig 11, it can be seen that the thrust increases linear with the increasing of current density when the current density is under 16A/mm2, then the thrust increases slowly as the effect of core saturation.

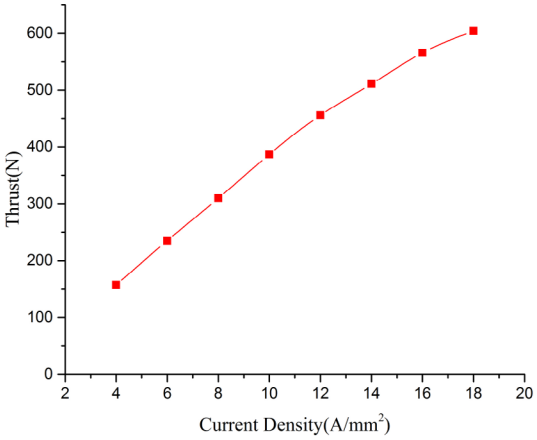

Figure 11. The thrust force characteristic with different current density.

5 Conclusion

A LVPM motor has been presented and described in this paper. FEA is employed to analyze the influence of the mover and stator pole number combination on the electromagnetic performance, such as the back EMF, the flux density, and the thrust ripple. The optimal stator/rotor pole pair for the maximum thrust is 1/11. Furthermore, the influence of design parameters including the slot opening ratio, the pole arc, and the magnet thickness on the torque capability has been investigated.It is found that the optimal pole arc for the maximum torque is around 0.81; and the optimal slot opening ratio is around 0.65. At last, it is worth to mention that these findings in this paper also can be easily extended and employed for the conventional rotate PMV motor designs.

References

1. A. Ishizaki, T. Tanaka, K. Takasaki, et al., Theory and optimum design of PM Vernier motor, International Conference on Electrical Machines and Drives, IET, 208-212 (1995)
2. A. Toba and T.A. Lipo, Generic torque-maximizing design methodology of surface permanent-magnet vernier machine, IEEE Transactions on Industry Applications, **36** (6), 1539-1546 (2000)
3. X. Li, K.T. Chau, and M. Cheng, Comparative analysis and experimental verification of an effective permanent-magnet Vernier machine, IEEE Transactions on Magnetics, **51** (7), 1-9 (2015)
4. D. Li, R. Qu, and T.A. Lipo, High power factor vernier permanent magnet machines, IEEE Transactions on Industry Applications, **50** (6), 1534-1540 (2013)
5. D.G. Dorrell, A.M. Knight, L. Evans, et al., Analysis and design techniques applied to hybrid vehicle drive machines-assessment of alternative IPM and induction motor topologies, IEEE Transactions on Industrial Electronics, **59** (10), 3690-3699 (2012)
6. I. Boldea, L.N. Tutelea, L. Parsa, et al., Automotive electric propulsion systems with reduced or no permanent magnets: an overview, IEEE Transactions on Industrial Electronics, **61** (10), 5696-5711 (2014)

7. W. Zhao, J. Zheng, J. Wang, et al., Design and analysis of a linear permanent- magnet vernier machine with improved force density, IEEE Transactions on Industrial Electronics, **63** (4), 1-1 (2015)
8. D. Li, R. Qu, J. Li, et al., Consequent pole, toroidal winding, outer rotor vernier permanent magnet machines, IEEE Transactions on Industry Applications, 1-1 (2015)
9. F. Magnussen and H. Lendenmann, Parasitic effects in PM machines with concentrated windings, IEEE Transactions on Industry Applications, **43** (5), 1223-1232 (2007)
10. S. Niu, K.T. Chau, J.Z. Jiang, et al., Design and control of a new double-stator cup-rotor permanent-magnet machine for wind power generation, IEEE Transactions on Magnetics, **43** (6), 2501-2503 (2007)
11. R. Qu, D. Li, and J. Wang, Relationship between magnetic gears and vernier machines, International Conference on Electrical Machines and Systems, IEEE, 1-6 (2011)
12. B. Kou, Y. Jin, L. Zhang, et al., Characteristic analysis and control of a hybrid excitation linear eddy current brake, Energies, **8** (7), 7441-7464 (2015)
13. K. Okada, N. Niguchi, and K. Hirata, Analysis of a vernier motor with concentrated windings, IEEE Transactions on Magnetics, **49** (49), 2241-2244 (2013)
14. S.L. Ho, S. Niu, and W.N. Fu, Design and comparison of vernier permanent magnet machines, IEEE Transactions on Magnetics, **47** (10), 3280-3283 (2011)
15. E. Barbisio, F. Fiorillo, and C. Ragusa, Predicting loss in magnetic steels under arbitrary induction waveform and with minor hysteresis loops, IEEE Transactions on Magnetics, **40** (4), 1810-1819 (2004)
16. M. Cheng, K.T. Chau, and C.C. Chan, Design and analysis of a new doubly salient permanent magnet motor, IEEE Transactions on Magnetics, **37** (4), 3012-3020 (2001)
17. Y. Du, M. Cheng, K.T. Chau, et al., Comparison of linear primary permanent magnet vernier machine and linear vernier hybrid machine, IEEE Transactions on Magnetics, **50** (11), 1-4 (2014)